Three-Dimensional TiO2 Film Deposited by ALD on Porous Metallic Scaffold for 3D Li-Ion Micro-Batteries: A Road towards Ultra-High Capacity Electrode

Maxime Hallot, David Troadec, Christophe Boyaval, Marielle Huve, Lotfi Benali Karroubi, Sai Patnaik, Thierry Brousse, Pascal Roussel, David Pech, Christophe Lethien

Three-Dimensional TiO_2 film deposited by ALD on porous metallic scaffold for 3D Li-ion micro-batteries: a road towards ultra-high capacity electrode

Maxime Hallot[1,2], Christophe Boyaval[1], David Troadec[1], Marielle Huvé[3], Lotfi Benali Karroubi[4], Sai Gourang Patnaik[4], Thierry Brousse[2,5], Pascal Roussel[3], David Pech[4*] and Christophe Lethien[1,2,6*]

[1] Institut d'Electronique, de Microélectronique et de Nanotechnologies, Université de Lille, CNRS, Université Polytechnique Hauts-de-France, UMR 8520 - IEMN, F-59000 Lille, France

[2] Réseau sur le Stockage Electrochimique de l'Energie (RS2E), CNRS FR 3459, 33 rue Saint Leu, 80039 Amiens Cedex, France

[3] Unité de Catalyse et de Chimie du Solide (UCCS), Université de Lille, CNRS, Centrale Lille, Université d'Artois, UMR 8181 – UCCS, F-59000 Lille, France

[4] LAAS-CNRS, Université de Toulouse, CNRS, 31400 Toulouse, France

[5] Institut des Matériaux Jean Rouxel (IMN), CNRS UMR 6502 – Université de Nantes, 2 rue de la Houssinière BP32229, 44322 Nantes cedex 3, France

[6] Institut Universitaire de France (IUF)

*Correspondence to: christophe.lethien@univ-lille.fr & dpech@laas.fr

KEYWORDS: TiO_2, thin films, high areal capacity, 3D Li-ion micro-batteries

ABSTRACT: To power the next generation of miniaturized electronic devices, the energy storage capability of Li-ion micro-batteries has to be significantly improved and the fabrication of high performance 3D electrodes is mandatory. Here we show how to carefully match the design of efficient 3D scaffold based on metallic porous template with the deposition parameters of titanium dioxide films made from thermal Atomic Layer Deposition method for designing efficient 3D electrodes for Li-ion micro-batteries. A 3D electrode made from Pt porous scaffold coated with 150 nm-thick anatase TiO_2 film reaches a high surface capacity value up to 1600 µAh.cm^{-2} at C/12 with a good cycling stability during 100 cycles.

TOC GRAPHIC:

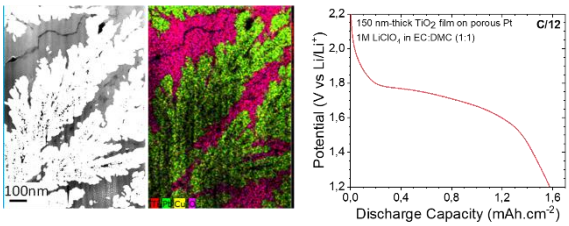

INTRODUCTION

Over the last decade, the number of connected electronic devices is in total expansion in our daily life through the Internet of Things concept for health, environmental or industrial monitoring, transportation, wearable electronics, and smart buildings[1,2]. Miniaturization of these intelligent systems opens the road to the next generation of IoT devices. A pertinent example of this groundbreaking technology is the Michigan Micro-Mote (M^3) designed and fabricated within the research group from David Blaauw[3]. In a restricted volume (1.5 mm^3), a miniaturized energy autonomous system embeds numerous sensors, a radiofrequency front-end, a data management unit and an energy harvesting and storage micro-source. The compactness of the M^3 was possible using advanced small form factor packaging methods such as 3D System-in-Package (3D SiP) technology which integrate, vertically or horizontally on the same substrate, many electronic functions including the miniaturized energy harvesting and storage sources. Integrated in an eye to follow the evolution of a glaucoma (i.e. the variation of the intraocular pressure within the eye), the transmission distance of the radiofrequency (RF) signal from the eye to a small data center is limited to ~ 10 cm (transmission of the signal in saline media (5 mm) and air). To get such smart microsystems autonomous and to increase the transmission distance of the RF signals (several tens of meters) in the frame of the IoT concept, lithium-ion micro-batteries and / or micro-supercapacitors with limited surface footprint and high storage capacity have to be used taking into account the limited available space. Consequently, footprint surface of the micro-battery is constrained, limiting the amount of active material and thus the energy performance.

A promising way to improve the energy performance of a Li-ion micro-battery consists of designing 3D devices where the active materials are deposited by step-

conformal deposition methods widely used in the semiconductor industry on high specific surface 3D scaffold. To tackle this issue, Atomic Layer Deposition technique remains the best deposition method to produce 3D Li-ion solid-state micro-batteries on large-scale wafers. Current collectors[4,5] (Pt, TiN), positive electrode[6–10] ($LiCoO_2$, $LiFePO_4$, $LiMn_2O_4$…), solid electrolyte[11–15] (Li_3PO_4, LIPON, $Li_7La_3Zr_2O_{12}$…) and negative electrodes[11,16–20] (TiO_2, V_2O_5, Nb_2O_5, $Li_4Ti_5O_{12}$…) have already been investigated as efficient thin films for all solid-state 3D Li-ion micro-battery. Among the existing functional electrodes made from ALD facility, bulk or nanostructured titanium dioxide is a promising alternative material to graphite and silicon based negative electrodes in a Li-ion battery owing to the low toxicity, low cost and safety issue. Within the numerous existing TiO_2 polymorphs, Rutile, Anatase, Brookite and TiO_2-B were widely studied[21–27]. With a mean potential around 1.7 V vs Li/Li^+ and a maximum theoretical gravimetric capacity of 335 $mAh.g^{-1}$ corresponding to the complete reduction of Ti^{4+} to Ti^{3+} (x_{Li}^+ = 1 mol Li^+ per TiO_2 molecule), titanium dioxide is a favorable electrode. Promising lithium insertion / extraction in TiO_2-(B) (x_{Li}^+=1) as well as TiO_2 anatase[21] polymorphs have already been reported at room temperature (x_{Li}^+ ~ 0.6)[21]. We have recently shown the fabrication of 155 nm-thick 3D TiO_2 electrode reaching more than 370 $\mu Ah.cm^{-2}$ at C/10 when cycled in liquid electrolyte. To reach this areal capacity value, an efficient 3D scaffold based on vertically etched silicon micro-tubes (with an area enhancement factor of 53) was coated with a TiO_2 film deposited by thermal ALD [11,26]. P. Vereecken *et al* have shown in 2017 the deposition of “doped” amorphous TiO_2 (with Chloride species) films on silicon micro-pillars using spatial Atomic Layer Deposition technique (s-ALD)[17]. The capacity of the amorphous TiO_2 electrode was close to 240 $\mu Ah.cm^{-2}$ at C/4 and 89 $\mu Ah.cm^{-2}$ at 20C but the galvanostatic discharge plot does not fit with the one expected for battery-

type material (flat plateau due to biphasic transition occurring during the lithiation/delithiation process). In that case, a quasi-triangular plot is observed as expected for pseudocapacitive material or nanostructured faradic materials[28] leading to fast rate capability.

In similar lines, many 3D porous metallic scaffolds have been reported in the past in the context of 3D micro-supercapacitors[29] and micro-batteries[30]. These porous current collectors are fabricated through ambient condition electrodeposition under sufficient cathodic overpotential in acidic media having appropriate metal salt precursors. The generated hydrogen bubbles create a Dynamic hydrogen bubble template (DHBT) for the reducing metal salt, thus resulting in a robust nanoporous dendritic structure with extremely high surface area. With variety of tunable parameters like reduction current, acid concentration, salt concentration etc. and low temperature aqueous fabrication, DHBT is a promising methodology for fabrication of 3D porous microelectrodes. Micrometer thick porous gold (Au-DHBT) and porous Pt/Cu (Pt-DHBT) electrodes can be easily produced through this technique having extremely high surface area.

Here we demonstrate the fabrication of TiO_2 electrode for 3D Li-ion micro-battery combining an efficient porous Pt scaffold with the Atomic Layer Deposition of 150 nm-thick anatase TiO_2 film. While the planar TiO_2 film shows a capacity close to 5 $\mu Ah.cm^{-2}$, a high areal capacity value (~ 1600 $\mu Ah.cm^{-2}$) is measured at C/12 for the 3D electrode. This areal capacity is ~ 4 times higher than the best capacities reached with thin film electrodes made from magnetron sputtering technique for planar Lithium-based micro-batteries[31–33] and ~ 6 times higher than the capacity reached by P. Vereecken *et al*[17] recently with 3D electrodes made from TiO_2 films thus validating the selected strategy of this study.

RESULTS AND DISCUSSION

As the deposition temperature is well known to be a critical issue to reach the desired TiO_2 polymorph (anatase), the porous metallic scaffold has to be carefully selected with specific surface and temperature stability point of view: in that case, porous gold and platinum scaffolds were investigated. A first approach was made with porous gold template coated with TiO_2 films. To study the temperature stability of the gold porous scaffold, thermal Atomic Layer Deposition of conformal TiO_2 films was achieved between 150 and 300 °C (**fig. S1**). The diffractograms of five samples deposited on planar Si / Pt substrate are shown in **fig. S1a**. The thickness of the five samples was close to ~ 100 nm. At 150 °C, the TiO_2 film seemed to be amorphous (or with so small crystallite size giving rise to the same XRD signature) as we did not observe any Bragg peaks coming from a TiO_2 phase and only two diffraction peaks (2θ = 40° and 46.5°) revealing the cubic phase of platinum layers (PDF 00-004-0802). From 175 up to 250 °C, the formation of the anatase polymorph (PDF 00-021-1272) was highlighted through the progressive increasing of the intensity of the Bragg peaks (~ 2θ = 25.5°, 37°, 38°, 38.5° and 48°). The Cyclic Voltammetry curves are reported in **fig. S1b** at 0.1 $mV.s^{-1}$ in 1M $LiClO_4$ EC / DMC electrolyte. As expected from the preliminary XRD study, the CV plot of the sample deposited at 150 °C exhibits no redox peaks and an electrochemical signature corresponding to the one of an amorphous compound. The CV curves of the planar TiO_2 samples deposited at substrate temperature ranging from 175 up to 300 °C exhibit two redox peaks at 1.7 and 2.2 V vs Li/Li^+ characteristic of the anatase TiO_2 polymorph[21]. Finally, the CV plot of the sample deposited at 300 °C shows a lower intensity than the sample deposited at 200 °C. From this preliminary combined XRD / CV study, we chose to set the deposition temperature close to 200 °C where the electrochemical

and structural analyses confirmed the formation of anatase polymorph. The morphological, structural and electrochemical analyses of 90 nm-thick TiO_2 film deposited at 200 °C on planar Si / Pt substrate are depicted in **fig. S2a-d**. While the SEM cross section image confirmed the dense nature of the 90 nm-thick TiO_2 film deposited by ALD (**fig. S2a**), the anatase polymorph was identified by XRD analysis (**fig. S2b**). From electrochemical point of view, the CV plots reported in **fig. S2c** at different sweep rates confirmed the intercalation / de-intercalation of the lithium ions in the anatase TiO_2 polymorph where two redox peaks are identified at ~ 1.7 V vs and 2.1 V Li/Li^+. Regarding the increasing of the sweep rate, we observed a shift of the reduction peak to lower potential value and toward higher potential for the oxidation peak as expected for battery-type electrode. From these CV curves, we extracted the b-coefficient[34] (**fig. S2d**) and confirmed that the charge storage mechanism within the TiO_2 film arises from a diffusion limited faradic process (b ~ 0.5).

Once the operating temperature of the Atomic Layer Deposition process was set to 200 °C to promote the formation of the anatase polymorph, we achieved the deposition of TiO_2 films on 3D porous gold scaffold. 90 nm-thick TiO_2 film was then deposited on 30 µm-depth 3D porous gold template. The porous gold framework had an apparent porosity of ~88% and aspect ratio, AEF (ratio between the electrochemical active surface area and the geometrical surface area) value of ~ 900 cm^2 per cm^2. This huge area to volume ratio thus ensures more active material loading per unit area of electrode and better interfacial kinetics as explained later in the CV studies after deposition of TiO_2 films by ALD. The resulting electrodeposited film is extremely porous and this can be observed in the scanning electron microscope (SEM) images (**fig. 1a**), where numerous gold dendrites and nodules are

extensively distributed in a cemented matrix. They are oriented in all directions, forming mechanically stable and self-supported pore walls. The morphological analysis is shown in **fig. 1a** before and after the TiO_2 deposition. From the SEM images, we observed that the ALD process did not significantly change the shape of the scaffold. The X-ray Diffraction analysis of the 3D electrode (3D Au / TiO_2) is depicted in **fig. 1b** where the two main peaks (at 2θ = 38° and 44°) are assigned to the porous gold template with a cubic structure (PDF file = 00-004-0784), while the two smaller other peaks, at 2θ = 25° and 48° were attributed to the anatase TiO_2 polymorph (PDF 00-021-1272) as expected. To check the beneficial effect issued from the 3D scaffold, two 90 nm-thick TiO_2 coatings, respectively 2D and 3D, were electrochemically tested in liquid electrolyte. The CV plots are reported in **fig. 1c** and both correspond to the electrochemical signature of a faradic electrode made from anatase TiO_2. Not surprisingly, the CV curve of the 3D Au / TiO_2 electrode exhibits a much higher current intensity meaning that the amount of active materials is greatly enhanced owing to the 3D template, as compared to the planar TiO_2 electrode. From these CVs, the areal capacities of the planar and 3D Au / TiO_2 electrodes were extracted and plotted vs the sweep rates (**fig. 1d**). While the planar electrode showed a surface capacity close to ~ 5 $\mu Ah.cm^{-2}$ at 0.1 $mV.s^{-1}$, the capacity of the 3D electrode reaches ~ 75 $\mu Ah.cm^{-2}$ at the same scan rate. As the sweep rates increases, the gap between the areal capacities of the planar and 3D electrodes progressively decreases due to the kinetic limitations of the lithium ions occurring within the TiO_2 film at high scan rate (diffusion-limited faradic process). The benefit from the 3D porous gold scaffold was then demonstrated but the enhancement of the surface capacity (~ x 15) did not correspond to the expected area enhancement factor of the 3D scaffold (AEF value = 900 cm^2 per cm^2) meaning that the ALD

process at 200 °C probably modified the behaviour of the 3D template. Indeed, we can infer that most of the porosity was not easily accessible by the ions coming from the electrolyte after the deposition process of the TiO_2 film at 200 °C reducing the AEF of the 3D scaffold. Consequently, we chose to move from porous gold metallic scaffold to the formation of platinum-based 3D template owing to the higher mechanical stability of porous Pt/Cu vs gold scaffolds. The relatively lower stability of porous Au matrix can be explained based on the very high surface diffusion coefficient of Au atoms (resulting in large number of defects, especially under the harsh deposition conditions) and high driving force to reduce its surface energy leading to coarsening of the dendritic structure, especially at high temperatures[35,36]. On the other hand, for Pt/Cu, Pt has much lower surface diffusion than Au while Cu aids in better adhesion and also prevents formation of larger particles, thus improving stability of the porous structure. The porous Pt/Cu scaffolds had extremely high surface area (AEF > 11 000) with high temperature stability (less than 20 % drop of the AEF value after annealing at 250 $^{\circ}$C). The evolution of the AEF value for Pt/Cu porous films increases with deposition time finally before levelling off at ~ 140 μm thickness (10 minutes of deposition).

To maximize the areal capacity of the TiO_2 electrode, both the area enhancement factor of the 3D scaffold and the thickness of active material were increased in the following section. Hence, 140 μm-depth 3D porous scaffold was coated with 150 nm-thick TiO_2 film deposited by ALD at 200 °C. A 150 nm-thick planar TiO_2 film was used as a reference sample to quantify the benefit from the 3D scaffold. In that case, the corresponding AEF value was approximately ~ 13 000. As the fabrication of the porous Pt scaffold came from the dealloying process of copper-platinum alloy, it was important to check the structural evolution of the 3D electrodes systematically during

the synthesis process. Several diffractograms are summarized in **fig. 2a**. While the platinum seed layer (green plot) exhibited a cubic structure (pdf file 00-004-0808) with two Bragg peaks occurring at 2θ = 40° and 46°, we observe broader peaks at similar 2theta angles assigned to Pt and an additional peak at 2θ = 41° attributed to CuPt mixed compounds (red diffractogram). The diffractogram of the 3D porous CuPt / TiO_2 electrode is also reported in the **fig. 2a** (blue curve) where the additional peaks are attributed the anatase polymorph deposited on the metallic CuPt scaffold by ALD at 200 °C. Raman spectroscopy analyses reported in **fig. 2b** confirmed that both 2D and 3D TiO_2 electrodes show the same structure: in that case, the main difference came from the shape of the metallic underlayer.

The morphological analyses of the planar and 3D electrodes are given in **fig. 2c-e**. The cross-section imaging of the 150 nm-thick planar TiO_2 film is shown in the panel I of the **fig. 2c**. As expected, the layer seems to be very dense and compact as typically observed for oxide films deposited by ALD. SEM top surface of the 3D porous sample is illustrated in the panels II (3D porous CuPt) and III (3D porous CuPt / TiO_2) where cauliflower-like morphology mixed with macropores (pore diameter ~ 50 µm) is observed. The DHBT deposition process is known to produce highly porous scaffold with hierarchical porosity. At the scale of the SEM images, we only observe the macroporosity. Meso and microporosities were then studied by TEM imaging. SEM cross-sectional imaging of the FIB-extracted 3D porous CuPt / TiO_2 sample is depicted in **fig. 2d**. The total thickness of the 3D scaffold is approximately 140 µm as shown in the inset of the **fig. 2d** (blue area). From this SEM analysis validating the porous shape of the template, we observed the large specific surface developed by the 3D scaffold that probably led to high surface capacity value of the 3D electrode. The chemical analysis of 3D porous CuPt / TiO_2 electrode was carried

out by Energy-dispersive X-ray spectroscopy (EDX) measurements at two different scales (at the micro and the nano scales) with both SEM and TEM analyses. As confirmed by EDX-SEM measurement (**fig. 2e**), the 3D metallic porous scaffold is composed by a CuPt metallic alloy (Pt:Cu / 74:26). As the Atomic Layer Deposition process is suitable to coat complex surface due to self-limiting reactions within the ALD reactor, the titanium and oxygen elements of the TiO_2 film are detected through the total thickness of the 3D scaffold, from the top to the bottom of the porous metallic template. EDX-TEM analyses are depicted in **fig. 2f** where a FIB lamella was prepared from a 3D porous CuPt / TiO_2 electrode. To protect the 3D electrode from the FIB preparation, an Al_2O_3 layer was deposited by ALD to fill the entire porosity of the electrode leading to a robust and protected sample.

The HRTEM images as well as the EDX maps highlight the cauliflower-like morphology of the CuPt alloy (**fig. 2f**) coated with TiO_2 active material. At the nanoscale, the pore-sizes vary between 6 to 18 nm, demonstrating the hierarchical porosity of metallic scaffold obtained by the DHBT process. The enlargement of the red and green area of the image of **fig. 2f III** reveals numerous crystalline nano-domains with inter fringe distances of 3.5 Å and 1.8 Å which can be attributed to the inter-planar spacing d_{101} of the TiO_2 anatase polymorph and d_{012} of the CuPt, respectively, in good agreement with the XRD study. The quantification of the TEM-EDX mapping (**fig. 2**) confirms also the CuPt and TiO composition of the scaffold and active layer, respectively.

Beside the morphological and structural analyses of our 150 nm-thick TiO_2 film deposited on 2D or 3D porous scaffold presented **fig.2**, it is important to compare the electrochemical performance of these electrodes made from either porous platinum scaffold or from porous gold template. The electrochemical characterizations were

achieved by Galvanostatic Charge / Discharge measurement in 1M $LiClO_4$ / EC / DMC at C/12. The discharges curves of both 2D and 3D electrodes are reported in **fig. 3a-b**. From the discharge plot of the planar sample, we observe a plateau at 1.8 V vs Li/Li^+ characteristic of a biphasic transition occurring during the intercalation mechanism of the lithium ions in the anatase TiO_2 structure. On one hand, the planar TiO_2 electrode (150 nm-thick) delivers a surface capacity close to ~ 5.8 $\mu Ah.cm^{-2}$ at C/12 (**fig. 3a**). On the other hand, the 3D TiO_2 electrode exhibit a very high surface capacity value close to 1600 $\mu Ah.cm^{-2}$. A plateau at 1.8V vs Li / Li+ was also observed in the discharge plot of the 3D electrode (**fig. 3b**). To discuss about the obtained performance, the following explanation is proposed. The bulk density of the TiO_2 anatase is 3.8 g cm^{-3}. If we consider the high density of the films deposited by ALD (~ 90 % of the theoretical one), the bulk density of TiO_2 films deposited by ALD method is about 3.4 g cm^{-3}. The thickness of the TiO_2 films (deposited on planar or 3D scaffold) is close to 150 nm thus leading to a low mass loading for the planar sample (~ 0.051 mg cm^{-2}). The theoretical gravimetric capacity of the bulk anatase TiO_2 is ~ 336 mAh g^{-1} for 1 Li^+ intercalation. Unfortunately, this capacity is usually limited to 174 mAh g^{-1} with ~ 0.5 Li^+ intercalation in TiO_2 except for nanometer-thick particles where nanosized effect[21] occurs thus leading to higher Li^+ per TiO_2. Regarding the mass loading of the 150 nm-thick TiO_2 film (0.051 mg cm^{-2}), the expected areal capacity is thus 8.9 $\mu Ah\ cm^{-2}$. Subsequently, the surface capacity value measured at C/12 on the 150 nm planar electrode (~ 5.8 $\mu Ah\ cm^{-2}$, figure 3a) corresponds to 113 mAh g^{-1}, i.e. 0.34 Li^+ per TiO_2. ALD method is one the best deposition technique suitable to perform the conformal deposition of thin films in range of 1 – 200 nm thickness. Consequently, no evolution of the film thickness would be expected if the deposition is carried out on planar substrate or 3D complex

scaffold meaning that the conformality is close to 100 %. In our case, the thickness of the TiO_2 layer deposited on 3D porous Pt template was evaluated close to 150 nm. As the surface capacity value of the 3D TiO_2 was measured to be close to 1600 µAh cm^{-2}, we clearly attribute the significant enhancement of the performance by the large specific surface of the 3D template associated to the conformal shape of thin films materials deposited by ALD.

In that case, the significant enhancement of the surface capacity value was demonstrated validating the selected strategy. Indeed, moving from gold to porous metallic scaffold allows maximising the capacity value based on an efficient template decorated with TiO_2 film deposited by ALD. The capacity retention of the planar and the 3D TiO_2 electrodes were also evaluated at C/12 during 100 cycles, and results are summarized in **fig. 3c.** The coulombic efficiency (CE) of 3D TiO_2 electrodes is plotted in **fig. 3d** and we observe that the CE stayed close to 100 % during 100 cycles. The GCD plot at the 50^{th} cycle is shown (**in the inset - fig. 3d**) to clearly highlight the stability performance of the 3D electrode.

Finally, the reached performance were benchmarked regarding state-of-the-art 3D electrodes reported in the literature (**fig. 3e**). In that respect, we plot the evolution of the surface capacity (in $mAh.cm^{-2}$) *vs* the thickness of active material. The nano-architectured templates based on Ni nanowires[37] and Al nanorods[38] were proposed ten years ago as efficient scaffold to improve the surface capacity of a TiO_2 film made by ALD. The spacing between two nanostructures (nanowire or nanorod) were kept low (~ 20 nm) and consequently, the thicknesses of active materials were limited by the spacing parameter. The surface capacity values of such 3D electrodes were approximately 10 and 160 $\mu Ah.cm^{-2}$ at C/10 for the Al nanorods and Ni nanowires respectively. In 2016, P. Notten *et al.* has reported the use of silicon micro-pillars

technology coated with a TiN current collector (made by ALD) and a 40 nm-thick TiO_2 film deposited by low pressure chemical vapour deposition technique (LP CVD)[39]. The normalized capacitance value of the 3D electrode was close to 200 $\mu Ah.cm^{-2}.\mu m^{-1}$. Regarding the thickness of the TiO_2 layer (40 nm), the areal capacity was approximately 8 $\mu Ah.cm^{-2}$. This "low capacity" value was attributed to the low area enhancement factor of the 3D template. This micro-architectured approach based on Si micropillars was improved by the group of P. Vereecken where TiO_2 films made by ALD technique were deposited on such 3D scaffold. In 2017, the deposition of “doped” amorphous TiO_2 (100 nm-thick) films on silicon micro-pillars using spatial-ALD[17] was reported. Similar results were proposed in 2019 when compared thermal ALD and s-ALD [40]. The capacity of the amorphous TiO_2 electrode was close to 240 $\mu Ah.cm^{-2}$ at C/4. In our group, we recently shown the fabrication of 155 nm-thick 3D TiO_2 electrode reaching more than 370 $\mu Ah.cm^{-2}$ at C/10. To reach this high areal capacity value, an original, robust, and highly efficient 3D scaffold based on vertically etched silicon micro-tubes (with an area enhancement factor of 53) was coated with a TiO_2 film (155 nm-thick) deposited by thermal ALD [11,26]. The results obtained in the frame of this study are implemented in this graph. With 150 nm-thick TiO_2 film deposited on porous platinum-based scaffold, the surface capacity value of the 3D electrode (~ 1.6 $mAh.cm^{-2}$) reaches a 10 times higher surface capacity value as compared to reported literature. More specifically, regarding the results obtained by the authors, this surface capacity value is 4.3 fold higher than the value reported[11] in 2017 by our group and 16 times higher than the capacity value reported by the group of P. Vereecken[40] in 2019. This is the highest capacity value reported up to now with such low amount of active material. When combined with a suitable positive electrode material[6,10] ($LiMn_2O_4$, $LiCoO_2$), such 3D TiO_2-based negative electrode could deliver

high energy density values, opening the way to high performance Li-ion micro-batteries for efficiently powering miniaturized electronics devices.

CONCLUSION

We demonstrate porous metallic scaffold decorated with TiO_2 thin film deposited by ALD as an attractive solution for designing 3D electrodes with ultra-high capacity values. In that respect, we show that porous gold scaffolds do not support the deposition temperature of the ALD process (200 °C) with areal capacity below 100 $\mu Ah.cm^{-2}$. Moving from gold to platinum porous-scaffold helps to tackle the temperature issue. The surface capacity of such 3D porous Pt / TiO_2 electrode reaches 1600 $\mu Ah.cm^{-2}$ at C/12, validating our strategy for designing efficient thin film electrodes for 3D Li-ion micro-batteries.

ACKNOWLEDGEMENT

This research is financially supported by the CNRS (INSIS department) within the 3D Li-ion micro-batteries project team between IEMN, LAAS, IMN and UCCS labs. The authors also want to thank the French network on electrochemical energy storage (RS2E) and the Store-Ex Labex for the support. The research is partially funded under the CASSIOPES ANR project. The French RENATECH network and the University of Lille are greatly acknowledged for the supporting the Center of MicroNanoFabrication (CMNF) facility. Chevreul Institute (FR 2638), Ministère de l'Enseignement Supérieur et de la Recherche, Région Hauts de France and FEDER are acknowledged for supporting and funding XRD and TEM facilities. D.P. acknowledges the support from the European Research Council (ERC-2017-CoG, Project 771793 3D-CAP).

DATA AVALAIBILITY

The raw/processed data required to reproduce these findings cannot be shared at this time as the data also forms part of an ongoing study.

COMPETING INTERESTS.

The authors declare no competing interests.

MATERIALS & CORRESPONDENCE.

Correspondence to Christophe Lethien & David Pech.

REFERENCES

(1) Lethien, C.; Le Bideau, J.; Brousse, T. Challenges and Prospects of 3D Micro-Supercapacitors for Powering the Internet of Things. *Energy Environ. Sci.* **2019**, *12* (1), 96–115. https://doi.org/10.1039/c8ee02029a.

(2) Raj, A.; Steingart, D. Review—Power Sources for the Internet of Things. *J. Electrochem. Soc.* **2018**, *165* (8), B3130–B3136. https://doi.org/10.1149/2.0181808jes.

(3) Chen, G.; Ghaed, H.; Haque, R. U.; Wieckowski, M.; Kim, Y.; Kim, G.; Fick, D.; Kim, D.; Seok, M.; Wise, K.; Blaauw, D.; Sylvester, D. A Cubic-Millimeter Energy-Autonomous Wireless Intraocular Pressure Monitor. *Dig. Tech. Pap. - IEEE Int. Solid-State Circuits Conf.* **2011**, 310–311. https://doi.org/10.1109/ISSCC.2011.5746332.

(4) Musschoot, J.; Xie, Q.; Deduytsche, D.; Van den Berghe, S.; Van Meirhaeghe, R. L.; Detavernier, C. Atomic Layer Deposition of Titanium Nitride from TDMAT Precursor. *Microelectron. Eng.* **2009**, *86* (1), 72–77. https://doi.org/10.1016/j.mee.2008.09.036.

(5) Fang, Q. Growth of Platinum Films by Atomic Layer Deposition (ALD). *White Pap. - Oxfor Instruments* **2009**, *44* (0), 1–8.

(6) Donders, M. E.; Arnoldbik, W. M.; Knoops, H. C. M.; Kessels, W. M. M.; Notten, P. H. L. Atomic Layer Deposition of LiCoO 2 Thin-Film Electrodes for All-Solid-State Li-Ion Micro-Batteries . *J. Electrochem. Soc.* **2013**, *160* (5), A3066–A3071. https://doi.org/10.1149/2.011305jes.

(7) Liu, J.; Banis, M. N.; Sun, Q.; Lushington, A.; Li, R.; Sham, T. K.; Sun, X.

Rational Design of Atomic-Layer-Deposited LiFePO4 as a High-Performance Cathode for Lithium-Ion Batteries. *Adv. Mater.* **2014**, *26* (37), 6472–6477. https://doi.org/10.1002/adma.201401805.

(8) Miikkulainen, V.; Ruud, A.; Østreng, E.; Nilsen, O.; Laitinen, M.; Sajavaara, T.; Fjellvaìšg, H. Atomic Layer Deposition of Spinel Lithium Manganese Oxide by Film-Body-Controlled Lithium Incorporation for Thin-Film Lithium-Ion Batteries. *J. Phys. Chem. C* **2014**, *118* (2), 1258–1268. https://doi.org/10.1021/jp409399y.

(9) Sheil, R.; Butts, D.; Jungjohann, K.; Yoo, J.; Dunn, B.; Chang, J. P. Plasma Enhanced Atomic Layer Deposition of Thin Film Li 1+x Mn 2−x O 4 for Realization of All Solid-State 3D Lithium-Ion Microbatteries . *J. Vac. Sci. Technol. A* **2021**, *39* (1), 012408. https://doi.org/10.1116/6.0000644.

(10) Hallot, M.; Nikitin, V.; Lebedev, O. I.; Retoux, R.; Troadec, D.; De Andrade, V.; Roussel, P.; Lethien, C. 3D LiMn 2 O 4 Thin Film Deposited by ALD: A Road toward High-Capacity Electrode for 3D Li-Ion Microbatteries . *Small* **2022**, *2107054*, 2107054. https://doi.org/10.1002/smll.202107054.

(11) Létiche, M.; Eustache, E.; Freixas, J.; Demortière, A.; De Andrade, V.; Morgenroth, L.; Tilmant, P.; Vaurette, F.; Troadec, D.; Roussel, P.; Brousse, T.; Lethien, C. Atomic Layer Deposition of Functional Layers for on Chip 3D Li-Ion All Solid State Microbattery. *Adv. Energy Mater.* **2017**, *7* (2), 1–12. https://doi.org/10.1002/aenm.201601402.

(12) Wang, B.; Liu, J.; Sun, Q.; Li, R.; Sham, T. K.; Sun, X. Atomic Layer Deposition of Lithium Phosphates as Solid-State Electrolytes for All-Solid-State Microbatteries. *Nanotechnology* **2014**, *25* (50), 504007.

https://doi.org/10.1088/0957-4484/25/50/504007.

(13) Kozen, A. C.; Pearse, A. J.; Lin, C. F.; Noked, M.; Rubloff, G. W. Atomic Layer Deposition of the Solid Electrolyte LiPON. *Chem. Mater.* **2015**, *27* (15), 5324–5331. https://doi.org/10.1021/acs.chemmater.5b01654.

(14) Nisula, M.; Shindo, Y.; Koga, H.; Karppinen, M. Atomic Layer Deposition of Lithium Phosphorus Oxynitride. *Chem. Mater.* **2015**, *27* (20), 6987–6993. https://doi.org/10.1021/acs.chemmater.5b02199.

(15) Kazyak, E.; Chen, K. H.; Wood, K. N.; Davis, A. L.; Thompson, T.; Bielinski, A. R.; Sanchez, A. J.; Wang, X.; Wang, C.; Sakamoto, J.; Dasgupta, N. P. Atomic Layer Deposition of the Solid Electrolyte Garnet Li7La3Zr2O12. *Chem. Mater.* **2017**, *29* (8), 3785–3792. https://doi.org/10.1021/acs.chemmater.7b00944.

(16) Eustache, E.; Tilmant, P.; Morgenroth, L.; Roussel, P.; Patriarche, G.; Troadec, D.; Rolland, N.; Brousse, T.; Lethien, C. Silicon-Microtube Scaffold Decorated with Anatase TiO2 as a Negative Electrode for a 3D Litium-Ion Microbattery. *Adv. Energy Mater.* **2014**, *4* (8), 1–11. https://doi.org/10.1002/aenm.201301612.

(17) Moitzheim, S.; Balder, J. E.; Poodt, P.; Unnikrishnan, S.; De Gendt, S.; Vereecken, P. M. Chlorine Doping of Amorphous TiO2 for Increased Capacity and Faster Li+-Ion Storage. *Chem. Mater.* **2017**, *29* (23), 10007–10018. https://doi.org/10.1021/acs.chemmater.7b03478.

(18) Liu, C.; Gillette, E. I.; Chen, X.; Pearse, A. J.; Kozen, A. C.; Schroeder, M. A.; Gregorczyk, K. E.; Lee, S. B.; Rubloff, G. W. An All-in-One Nanopore Battery Array. *Nat. Nanotechnol.* **2014**, *9* (12), 1031–1039.

https://doi.org/10.1038/nnano.2014.247.

(19) Ouendi, S.; Arico, C.; Blanchard, F.; Codron, J. L.; Wallart, X.; Taberna, P. L.; Roussel, P.; Clavier, L.; Simon, P.; Lethien, C. Synthesis of T-Nb2O5 Thin-Films Deposited by Atomic Layer Deposition for Miniaturized Electrochemical Energy Storage Devices. *Energy Storage Mater.* **2019**, *16* (August), 581–588. https://doi.org/10.1016/j.ensm.2018.08.022.

(20) Meng, X.; Liu, J.; Li, X.; Banis, M. N.; Yang, J.; Li, R.; Sun, X. Atomic Layer Deposited Li4Ti5O12 on Nitrogen-Doped Carbon Nanotubes. *RSC Adv.* **2013**, *3* (20), 7285–7288. https://doi.org/10.1039/c3ra00033h.

(21) Wagemaker, M.; Mulder, F. M. Properties and Promises of Nanosized Insertion Materials for Li-Ion Batteries. *Acc. Chem. Res.* **2013**, *46* (5), 1206–1215. https://doi.org/10.1021/ar2001793.

(22) Ellis, B. L.; Knauth, P.; Djenizian, T. Three-Dimensional Self-Supported Metal Oxides for Advanced Energy Storage. *Adv. Mater.* **2014**, *26* (21), 3368–3397. https://doi.org/10.1002/adma.201306126.

(23) Tesfaye, A. T.; Sopha, H.; Ayobi, A.; Zazpe, R.; Rodriguez-Pereira, J.; Michalicka, J.; Hromadko, L.; Ng, S.; Spotz, Z.; Prikryl, J.; Macak, J. M.; Djenizian, T. TiO2 Nanotube Layers Decorated with Al2O3/MoS2/Al2O3 as Anode for Li-Ion Microbatteries with Enhanced Cycling Stability. *Nanomaterials* **2020**, *10* (5). https://doi.org/10.3390/nano10050953.

(24) Wang, J.; Polleux, J.; Brezesinski, T.; Tolbert, S.; Dunn, B. The Pseudocapacitive Behavior of TiO2 (Anatase) Nanoparticles. *ECS Trans.* **2008**, *11* (31), 101–111.

(25) Gerasopoulos, K.; Chen, X.; Culver, J.; Wang, C.; Ghodssi, R. Self-Assembled Ni/TiO2 Nanocomposite Anodes Synthesized via Electroless Plating and Atomic Layer Deposition on Biological Scaffolds. *Chem. Commun.* **2010**, *46* (39), 7349–7351. https://doi.org/10.1039/c0cc01689f.

(26) Eustache, E.; Tilmant, P.; Morgenroth, L.; Roussel, P.; Patriarche, G.; Troadec, D.; Rolland, N.; Brousse, T.; Lethien, C. Silicon-Microtube Scaffold Decorated with Anatase TiO2 as a Negative Electrode for a 3D Litium-Ion Microbattery. *Adv. Energy Mater.* **2014**, *4* (8), 1–11. https://doi.org/10.1002/aenm.201301612.

(27) Bach, S.; Pereira-Ramos, J. P.; Willman, P. Investigation of Lithium Diffusion in Nano-Sized Rutile TiO2 by Impedance Spectroscopy. *Electrochim. Acta* **2010**, *55* (17), 4952–4959. https://doi.org/10.1016/j.electacta.2010.03.101.

(28) Simon, P.; Gogotsi, Y.; Dunn, B. And Supercapacitors Begin ? *Science (80-.).* **2014**, *343* (March), 1210–1211.

(29) Ferris, A.; Garbarino, S.; Guay, D.; Pech, D. 3D RuO2 Microsupercapacitors with Remarkable Areal Energy. *Adv. Mater.* **2015**, *27* (42), 6625–6629. https://doi.org/10.1002/adma.201503054.

(30) Patnaik, S. G.; Jadon, A.; Tran, C. C. H.; Estève, A.; Guay, D.; Pech, D. High Areal Capacity Porous Sn-Au Alloys with Long Cycle Life for Li-Ion Microbatteries. *Sci. Rep.* **2020**, *10* (1), 1–8. https://doi.org/10.1038/s41598-020-67309-7.

(31) Hallot, M.; Demortière, A.; Roussel, P.; Lethien, C. Sputtered LiMn1.5Ni0.5O4 Thin Films for Li-Ion Micro-Batteries with High Energy and Rate Capabilities.

Energy Storage Mater. **2018**, *15* (August), 396–406. https://doi.org/10.1016/j.ensm.2018.08.012.

(32) Hallot, M.; Caja-munoz, B.; Leviel, C.; Lebedev, O. I.; Retoux, R.; Avila, J.; Roussel, P.; Asensio, M. C.; Lethien, C. Atomic Layer Deposition of a Nanometer-Thick Li 3 PO 4 Protective Layer on LiNi 0 . 5 Mn 1 . 5 O 4 Films : Dream or Reality for Long-Term Cycling ? **2021**. https://doi.org/10.1021/acsami.0c21961.

(33) Navone, C.; Tintignac, S.; Pereira-Ramos, J. P.; Baddour-Hadjean, R.; Salot, R. Electrochemical Behaviour of Sputtered C-V2O5 and LiCoO2 Thin Films for Solid State Lithium Microbatteries. *Solid State Ionics* **2011**, *192* (1), 343–346. https://doi.org/10.1016/j.ssi.2010.04.023.

(34) Augustyn, V.; Simon, P.; Dunn, B. Pseudocapacitive Oxide Materials for High-Rate Electrochemical Energy Storage. *Energy Environ. Sci.* **2014**, *7* (5), 1597–1614. https://doi.org/10.1039/c3ee44164d.

(35) Snyder, J.; Asanithi, P.; Dalton, A. B.; Erlebacher, J. Stabilized Nanoporous Metals by Dealloying Ternary Alloy Precursors. *Adv. Mater.* **2008**, *20* (24), 4883–4886. https://doi.org/10.1002/adma.200702760.

(36) Cherevko, S.; Kulyk, N.; Chung, C. H. Nanoporous Pt@Au XCu 100-x by Hydrogen Evolution Assisted Electrodeposition of Au XCu 100-x and Galvanic Replacement of Cu with Pt: Electrocatalytic Properties. *Langmuir* **2012**, *28* (6), 3306–3315. https://doi.org/10.1021/la203625e.

(37) Wang, W.; Tian, M.; Abdulagatov, A.; George, S. M.; Lee, Y. C.; Yang, R. Three-Dimensional Ni/TiO 2 Nanowire Network for High Areal Capacity Lithium

Ion Microbattery Applications. *Nano Lett.* **2012**, *12* (2), 655–660. https://doi.org/10.1021/nl203434g.

(38) Cheah, S. K.; Perre, E.; Rooth, M.; Fondell, M.; Hårsta, A.; Nyholm, L.; Boman, M.; Lu, J.; Simon, P.; Edstro, K. Nanoelectrodes for Microbattery Applications. *Nano Lett.* **2009**, *9* (9), 3230–3233.

(39) Xie, J.; Oudenhoven, J. F. M.; Li, D.; Chen, C.; Eichel, R.-A.; Notten, P. H. L. High Power and High Capacity 3D-Structured TiO 2 Electrodes for Lithium-Ion Microbatteries . *J. Electrochem. Soc.* **2016**, *163* (10), A2385–A2389. https://doi.org/10.1149/2.1141610jes.

(40) Moitzheim, S.; Balder, J. E.; Ritasalo, R.; Ek, S.; Poodt, P.; Unnikrishnan, S.; De Gendt, S.; Vereecken, P. M. Toward 3D Thin-Film Batteries: Optimal Current-Collector Design and Scalable Fabrication of TiO2 Thin-Film Electrodes. *ACS Appl. Energy Mater.* **2019**, *2* (3), 1774–1783. https://doi.org/10.1021/acsaem.8b01905.

(41) Létiche, M.; Hallot, M.; Huvé, M.; Brousse, T.; Roussel, P.; Lethien, C. Tuning the Cation Ordering with the Deposition Pressure in Sputtered LiMn1.5Ni0.5O4 Thin Film Deposited on Functional Current Collectors for Li-Ion Microbattery Applications. *Chem. Mater.* **2017**, *29* (14), 6044–6057. https://doi.org/10.1021/acs.chemmater.7b01921.

(42) Arico, C.; Ouendi, S.; Taberna, P. L.; Roussel, P.; Simon, P.; Lethien, C. Fast Electrochemical Storage Process in Sputtered Nb2O5 Porous Thin Films. *ACS Nano* **2019**, *13* (5), 5826–5832. https://doi.org/10.1021/acsnano.9b01457.

(43) Gerasopoulos, K.; Pomerantseva, E.; McCarthy, M.; Brown, A.; Wang, C.;

Culver, J.; Ghodssi, R. Hierarchical Three-Dimensional Microbattery Electrodes Combining Bottom-up Self-Assembly and Top-down Micromachining. *ACS Nano* **2012**, *6* (7), 6422–6432. https://doi.org/10.1021/nn301981p.

(44) Cheah, S. K.; Perre, E.; Rooth, M.; Fondell, M.; Hårsta, A.; Nyholm, L.; Boman, M.; Gustafsson, T.; Lu, J.; Simon, P.; Edström, K. Self-Supported Three-Dimensional Nanoelectrodes for Microbattery Applications. *Nano Lett.* **2009**, *9* (9), 3230–3233. https://doi.org/10.1021/nl9014843.

METHODS

Fabrication of the 3D Porous Au and Pt scaffolds. For 3D porous Au, a Ti (100 nm) / Au (300 nm) thin film was deposited by evaporation on an oxidized silicon substrate and electrochemically pretreated by cycling the potential at a scan rate of 100 $mV.s^{-1}$ between -0.3 and +1.7 V versus saturated calomel electrode (SCE) in 1 M H_2SO_4 until a stable voltammogram was obtained. Porous metallic current collectors were prepared using the DHBT technique from an optimized solution of 2 x 10^{-3} M of $HAuCl_4.3H_2O$ in 3 M H_2SO_4 by applying 5 $A.cm^{-2}$ for 20 min in a 3-electrode configuration. For 3D porous Pt/Cu, A Ti (50 nm) / Pt (200 nm) thin film was deposited by evaporation on an oxidized silicon substrate and used as working electrode, saturated calomel electrode (SCE) as reference electrode and a Pt mesh as counter electrode followed by two CV cycles between -0.6 to +1.2 *vs.* SCE to facilitate better nucleation. Porous metallic current collectors were then prepared using a similar DHBT technique from an optimized solution of 30 mM H_2PtCl_6 and 15mM $CuSO_4.5H_2O$ in 1 M H_2SO_4 by applying 6.5 $A.cm^{-2}$ for 10 min in a 3-electrode configuration. Cu was further de-alloyed electrochemically though cyclic voltammetry in 0.5M H_2SO_4 between -0.38 to +1.2 V vs SCE for 50 cycles at 10 $mV.s^{-1}$.

Atomic Layer Deposition (ALD) of TiO_2 films. The TiO_2 films were deposited by ALD on a planar substrate composed of stacked Al_2O_3 / Pt layers on a silicon wafer as already reported by our group in previous publications[11,31,41,42]. The TiO_2 films (90 and 150 nm-thick) were deposited by atomic layer deposition method from a TFS200 Beneq ALD reactor; this technique ensures a conformal deposit on the 3D scaffold. The precursors for the TiO_2 ALD were $TiCl_4$ and H_2O. The TiO_2 ALD reactions are supposed to be :

1. $TiCl_4$ adsorption with some HCl release

2. $TiCl_{3\text{-}ads} + H_2O \rightarrow TiO_2 + HCl_{(g)}$

The TiO_2 canister was not heated as it operates at high vapor pressure. The substrate holder temperature was varied between 150 and 300 °C in order to study the polymorphism of the TiO_2 films. The deposition reaction was achieved in four steps, each precursor being introduced separately, with a nitrogen purge of 300 sccm between two cycles. The growth rate of the TiO_2 anatase polymorph was 0.8 Å per ALD cycle at 200 °C.

Morphological and chemical analyses of TiO_2 films. For 3D films, thicknesses and EDX analyses were evaluated by Scanning Electron Microscopy technique (Zeiss Ultra 55 Scanning Electron Microscope). Structural properties were examined by X-ray diffraction using a Rigaku Smarlab diffractometer in Bragg-Brentano mode employing Cu Kα-radiation (λ = 1.5418 Å). An offset of 2° was applied on the silicon substrate to avoid the high intensity of the (100) silicon peak. TEM measurements were conducted on a S/TEM FEI TITAN Themis 300 equipped with a probe corrector for a resolution of 0.6 Å in STEM mode, an electron monochromator for an energy resolution of 140 meV, and a Super-X quad EDS detector for elemental analysis. The microscope has several annual detectors for imaging, and a post-column GATAN Quantum ERS/966 GIF operating a dual EELS mode.

Electrochemical characterizations. Cyclic voltammetry (CV) and Galvanostatic Charge and Discharge Plots were investigated on a VMP3 potentiostat/galvanostat equipment using a homemade Teflon like flat-cell with Li metal used as the counter and reference electrode. The electrolyte (1 mL), comprising 1 M $LiClO_4$, dissolved in ethylene carbonate (EC) and diethylene carbonate (DEC) in a 1:1 ratio, was poured into the flat-cell cavity. The tested area (circular shape) of the sample was limited to

0.4 cm^2. The flat cells under test were placed in a glove box with controlled atmosphere (O_2 and H_2O quantities: less than 1 ppm).

LIST OF THE FIGURES AND FIGURE CAPTIONS

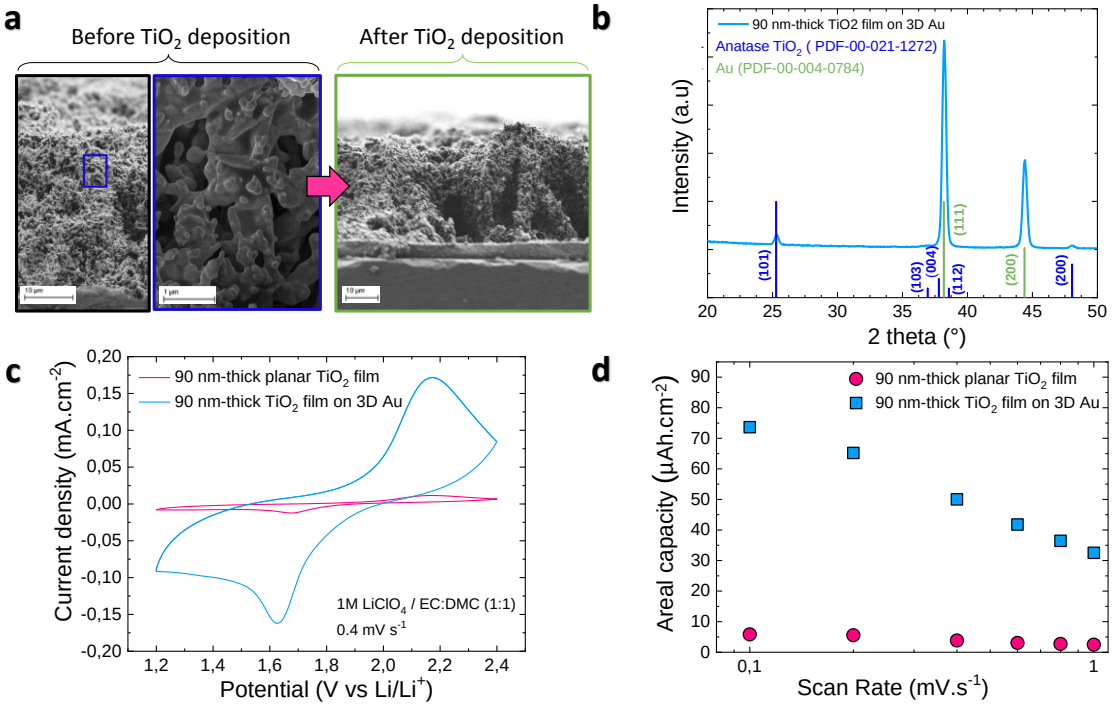

Fig. 1 | Preliminary studies on 3D porous gold metallic scaffold. a. Scanning Electron Microscope imaging of porous gold collector before and after the TiO_2 deposition by ALD at 200 °C. **b.** X-Ray Diffraction analysis of the 90 nm-thick TiO_2 film deposited on porous gold scaffold. **c.** CV profile of 90 nm-thick TiO_2 film deposited on planar Si wafer and 3D porous gold template. **d.** Evolution of the areal capacity vs the scan rate for 2D and 3D samples.

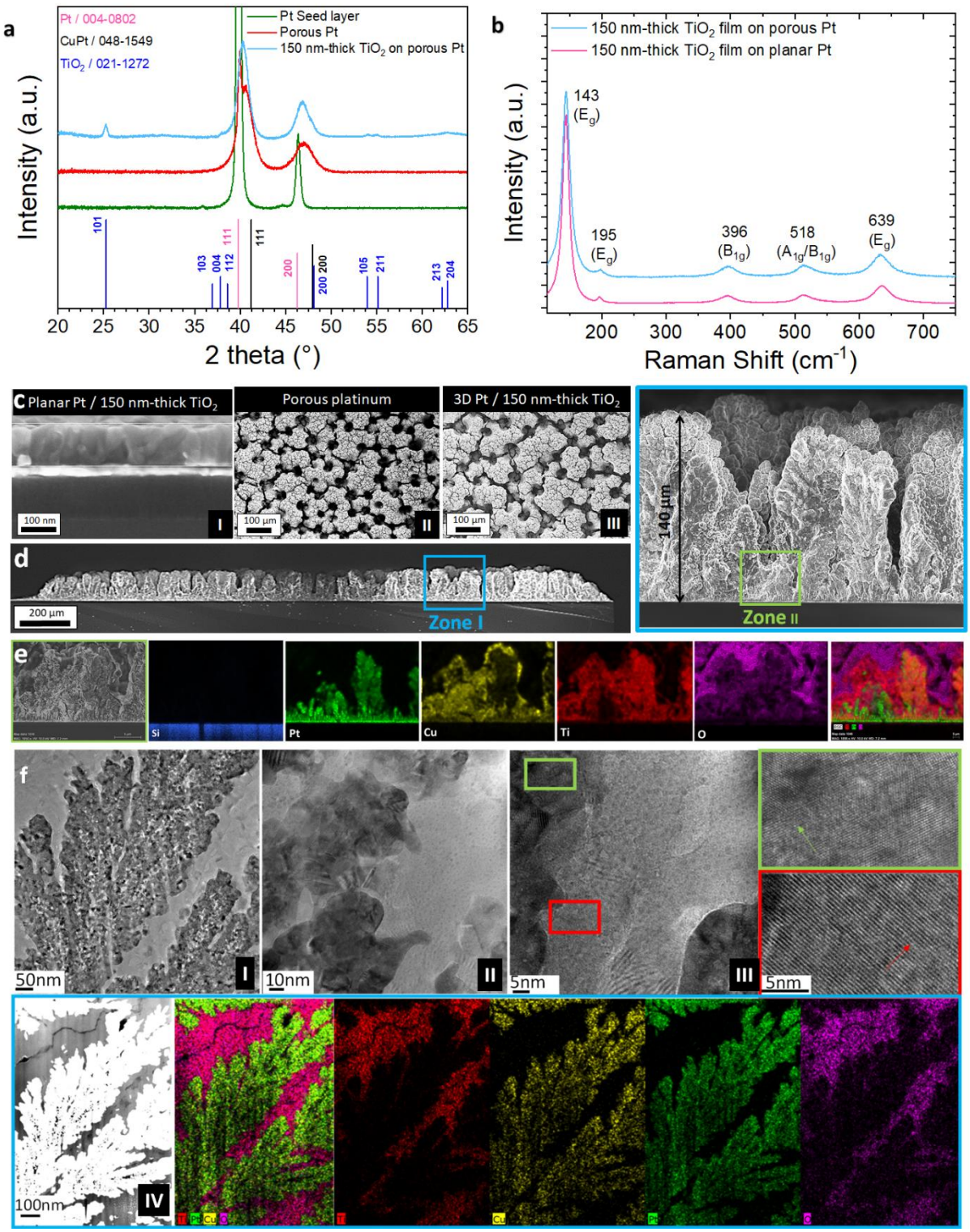

Fig. 2 | Structural and morphological analyses of the 150 nm-thick TiO_2 film deposited on planar Si / Pt substrate and on the porous platinum 3D scaffold. **a.** Diffractogramms of the Pt seed layers, porous Pt scaffold and the TiO_2 film deposited on to 3D metallic template. **b.** Raman analyses of the TiO_2 films deposited

on planar Si wafer and a 3D scaffold. **c-e.** Scanning electron microscope imaging (top view and cross-sections). **f.** TEM analyses performed on 3D porous metallic scaffold decorated with a 150 nm-thick TiO_2 film. Panels I-II-III: TEM images for increasing magnification. magnification of the green and red area of III. Panel IV HAADF image and corresponding EDX map

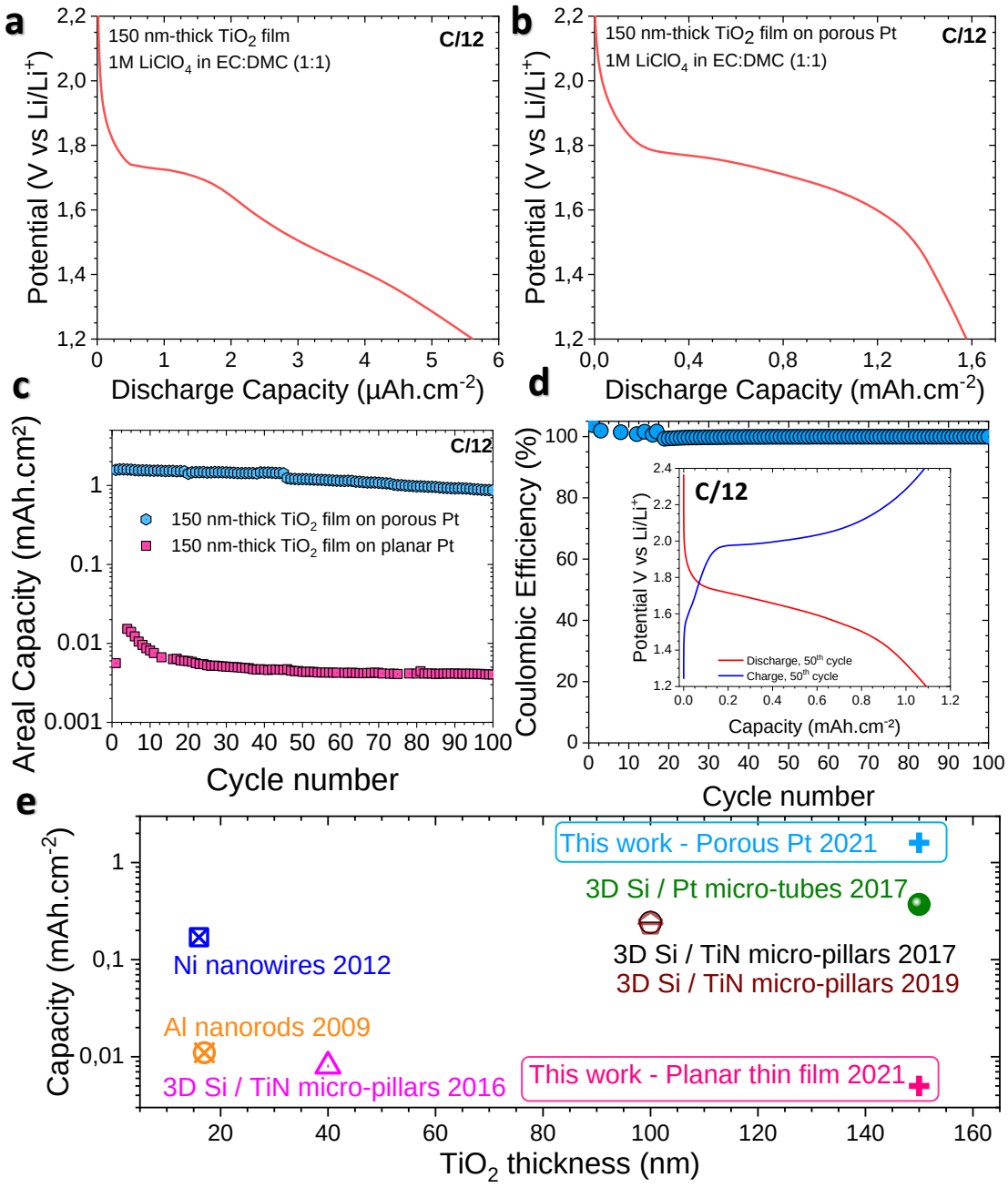

Fig. 3 | Electrochemical performance of the 3D TiO_2 electrode. a. Galvanostatic Discharge capacity of 150 nm-thick TiO_2 thin film deposited on Pt coated-planar Si wafer at C/12. **b.** Galvanostatic Discharge capacity of 150 nm-thick TiO_2 thin film deposited on 3D platinum porous scaffold. **c.** Evolution of the discharge capacity of the planar and 3D TiO_2 films at C/12 vs the number of cycles. **d.** Coulombic efficiency of the 3D TiO2 electrode (150 nm-thick TiO2 film deposited on porous Pt scaffold). The Galvanostatic Charge/Discharge (GCD) curves at the 50th cycle are presented in

the inset. **e.** Benchmarking of this work regarding the existing 3D TiO_2 electrodes for high performance Li-ion micro-battery[11,16,17,39,40,43,44].